Check for updates

NY-ESO-1 antigen-antibody interaction process based on an TFBG plasmonic sensor

HANG QU,[1] LINYAO TAN,[1] FANG-CAI WU,[2] WEIYUAN HUANG,[1] KAIWEI LI,[3] XIAOYONG CHEN,[4,7] YI-WEI XU,[5,8] AND XUEHAO HU[6]

[1]*Research Center for Advanced Optics and Photoelectronics, Department of Physics, College of Science, Shantou University, Shantou, Guangdong 515063, China*
[2]*Department of Radiation Oncology, Cancer Hospital of Shantou University Medical College, Shantou 515041, Guangdong, China*
[3]*Key Laboratory of Bionic Engineering of Ministry of Education, Jilin University, Changchun, China*
[4]*School of Electrical Engineering and Intelligentization, Dongguan University of Technology, Dongguan 523808, China*
[5]*Department of Clinical Laboratory Medicine, Cancer Hospital of Shantou University Medical College, Shantou 515041, Guangdong, China*
[6]*Department of Electromagnetism and Telecommunication, University of Mons, Boulevard Dolez 31, 7000 Mons, Belgium*
[7]*xychen@dgut.edu.cn*
[8]*yiwei512@126.com*

Abstract: Autoantibodies against New York esophageal squamous cell cancer 1 (NY-ESO-1) play a crucial role in the diagnosis of esophageal cancer. In this work, a surface plasmonic tilted fiber Bragg grating (TFBG) biosensor is proposed for the detection of NY-ESO-1 antibody, as well as the investigation of the hook effect (which refers to the false negative result in some immunoassays when the concentration of antibodies in the sample is very high) during biomolecular binding between NY-ESO-1 antigen and antibody. The biosensor is made by an 18° TFBG coated with a 50-nm-thick gold film over the fiber surface together with NY-ESO-1 antigens attached to the metallic surface serving as bio-receptors. This biosensor can provide a limit of detection at a concentration of 2×10^{-7} µg/ml with a good linearity in the range from 2×10^{-7} to 2×10^{-5} µg/ml. For a concentration higher than 2×10^{-3} µg/ml, the performance of the sensor probe is reduced owing to the hook effect. Furthermore, experimental results have also demonstrated the repeatability of the proposed biosensor. This proposed biosensor features label-free, compactness, and fast response, which could be potentially applied in the diagnosis of esophageal cancer.

1. Introduction

Esophageal cancer is the sixth most common cause of cancer death worldwide and has a significant impact on public health. In the Asia-Pacific region, the dominant disease phenotype is esophageal squamous cell carcinoma (ESCC), which is attributed to the prevalence of smoking, alcohol, and betel nut chewing [1]. Although there are some methods that use interdisciplinary methods to treat esophageal cancer, the results are still not good [2]. At present, surgery is the first choice for the treatment of esophageal squamous cell cancer [3], but due to the lack of early diagnosis techniques, many patients are diagnosed at an advanced stage and missed the best treatment opportunity. Thus, highly sensitive and selective techniques that enable early detection of cancer cells are requisite in cancer diagnostics [1]. However, during the early stages of cancer development, the number of cancer cells available for detection is very limited, and serum markers are not sufficiently sensitive for early diagnostic purposes [4].

Autoantibodies represent a stable and amplified signature of the anti-tumour immune response that may be generated prior to the clinical detection of other tumour proteins and prior to the first clinically detectable signs of cancer or its recurrence [5]. Thus, there is great interest in using autoantibodies as diagnostic and prognostic blood-based biomarkers. According to current evidence, tumor-associated autoantibodies (TAAs) show promise as blood-based markers for early warning of ESCC. It is speculated that TAA production is triggered by increased immunogenicity of corresponding antigens, such as proteins which are mutated, aberrantly expressed, misfolded or overexpressed in the early stages of carcinogenesis [6]. In addition, several properties of TAAs allow their application as early-warning biomarkers, including stability, accessibility in blood specimens, and detectability which sometimes precedes clinical diagnosis by several months to years [7]. New York esophageal squamous cell cancer 1 (NY-ESO-1) has been reported in esophageal carcinoma [8]. As an important member of cancer/testes antigens (CTA), NY-ESO-1 plays a crucial role in the treatment and prognosis of esophageal carcinoma [9] and has previously been shown to induce autoantibodies in esophageal cancer [10,11]. A variety of methods have been developed for the detection of autoantibodies against NY-ESO-1, such as enzymatic immunoassay EIA/ELISA. ELISA has been widely used for specific detection of a wide variety of target analytes in different kinds of samples; however, it has certain limitations such as a tedious/laborious assay procedure and an insufficient level of sensitivity in bio-recognition of challenging biomolecular entities [12].

Optical fiber sensors, especially tilted fiber Bragg gratings (TFBGs), have many advantages, such as small size, electromagnetic immunity, and high refractometric sensitivity, which have been extensively studied for biomedical detection of analytes at low concentrations [13,14]. A TFBG has a core mode and multiple cladding modes. The latter feature a high-density comb-like transmitted spectrum with narrow banded resonances (Q-factor $\sim 10^4$), providing outstanding sensitivity and a low limit of detection (LOD) for biomedical detection [15]. To further improve the refractometric sensitivities, TFBGs can be metal-coated to generate surface Plasmon resonance (SPR) [16]. The upgraded optical fiber sensor with high-precision has become a popular choice for biochemical sensors for specific molecular recognition by coating sensitive biofilm outside the active metal deposition layer. By monitoring and recording the transmission spectral resonance of the TFBG-SPR biomolecular probe sensor, the combination of biosensitive membranes and specific biomolecules can be dynamically understood. In addition, we can infer whether the analyzers contain some specific biomolecules according to the specificity of biomolecules [17]. In the past few years, TFBG-SPR sensor probes have been widely studied for biochemical sensing. In 2020, Loyez et al. proposed an all-fiber plasmonic aptasensor for the detection of circulating tumor cells (CTCs) with a LOD of 49 cells/mL [18]. In 2021, Liu et al. demonstrated a plasmonic optical fiber biosensing platform for the ultrasensitive detection of environmental estrogens by estrogen receptor, showing a LOD of 1.5×10^{-3} ng/ml [19]. In 2022, Chen et al. proposed a plasmonic TFBG-SPR sensor immobilized with a specific antibody against GPR30 (an intracellular seven-transmembrane G protein-coupled estrogen receptor), which could detect breast cancer cells in concentration of 5 cells/mL within 20 minutes [20].

Inspired by the high refractive index sensitivity of TFBG-SPR sensor probes and the high specificity of the NY-ESO-1 antibody for the esophageal cancer cells autoimmune cancer/testis antigen NY-ESO-1 [21], we proposed and demonstrated a label-free biosensor for the detection of NY-ESO-1 antibody. It is found that our biosensor can provide a LOD at a concentration of 2×10^{-7} µg/ml, and with good linearity in the measured range from 2×10^{-7} to 2×10^{-5} µg/ml. As a hook effect was observed when the NY-ESO-1 antibody concentration is higher than 2×10^{-3} µg/ml, the effective measurable range of our biosensor is limited to 2×10^{-7}- 2×10^{-3} µg/ml. The excellent performance and its simple structure, simple preparation, and small size make the sensor proposed in this paper a good choice for in situ, label-free, early, and subscale detection (interactions of organisms at the nanoscale) of cancer cells.

2.   Materials and methods

2.1.   Materials

The phosphate buffer saline (PBS) was purchased from Beijing Solarbio Science & Technology Co., Ltd., Beijing, China. The 11-mercapto-undecanoic acid (11-MUA), 1-ethyl(3-dimethylaminopropyl)-carbodiimide (EDC) and N-hydroxy-succinimide (NHS) were purchased from Hefei Bomei Biological Engineering Company, Anhui, China. The bovine serum albumin (BSA) was purchased from Shanghai Aladdin biological technology Co., Ltd., Shanghai, China. The NY-ESO-1 antibody (E978): sc-53869 (200µg/ml) were provided by SANTA CRUZ BIOTECHNOLOGY, INC, and autoimmunogenic cancer/testis antigen (aCTA) NY-ESO-1 were prepared by Shantou University Medical College, Shantou, China [4]. The antigen, antibody and BSA solution used in the experiment were all diluted in PBS solution. The optical fiber (F-SM1500-4.2/125) used for the TFBG inscription was purchased from Newport Opto-Electronics Technologies (Wuxi) Co., Ltd., Wuxi, China, with highly germanium doped in the fiber core.

2.2.   Fabrication of the TFBG with gold coating

The TFBGs used in this work were inscribed by scanning phase mask (as Fig. 1 shows) technique in a single-mode fiber with a germanium-doped core. The fiber was placed very close behind the phase mask, and a 193 nm pulsed beam from the ArF excimer laser (3 mJ and 200 Hz) was focused on the fiber core. The TFBG features a length of ~4 mm, a period of 0.559 µm, and a tilt angle of 18°.

In the TFBG spectrum, the positions of core mode resonance (λ_B) and cladding mode resonances (λ_{clad}^i) can be expressed as follows:

$$\lambda_B = 2n_{eff,core}\Lambda$$

$$\lambda_{clad}^i = (n_{eff,core} + n_{eff,clad}^i)\Lambda$$

where λ_B represents the Bragg wavelength of the core mode, λ_{clad}^i represents the wavelengths of the cladding modes, and Λ represents the grating period along the fiber. $n_{eff,core}$ and $n_{eff,clad}^i$ are the effective indices of the core mode and the cladding mode with a mode number of i, respectively. Afterward, a gold film with a thickness of approximately 50 nm was deposited over the fiber surface using a magnetron sputtering coater (SD-900 M, Beijing Boyuan Micro-nano Technology Co.). After that, the gold-coated TFBGs were annealed for 2 h at ~200 °C to enhance the adhesion of the gold film to the silica surface [22]. Surface plasmon wave (SPW) can be excited when the phase matching condition is met. Therefore, the TFBG-SPR sensor is highly sensitive to the surrounding environment and can be used for biomolecular detection. Additionally, it should be noted that the incident light has to be in the P-polarization state, enabling power coupling to occur between the TFBG-excited cladding modes and the SPW.

### 2.3.   Bio-functionalization of the metallic surface

To realize the specific detection of the NY-ESO-1 antibody, surface functionalization was carried out for the plasmonic TFBG. In this work, the aCTA NY-ESO-1 was bonded on the metallic surface serving as bio-detectors, as shown in Fig. 2. The surface functionalization includes three steps as follows:

First, the plasmonic TFBG biosensor was rinsed several times with ethanol and with Milli-Q water for removing the unwanted contaminants on the metallic surface, and then it was immersed in the 11-MUA solution (0.8 mM, dissolved in anhydrous ethanol) for 10 hours to generate a self-assembly of a monolayer of mercapto compounds on the metallic surface.

Second, the sensor was again rinsed with ethanol and with Milli-Q water for removing the unconnected 11-MUA, and then it was immersed in a mixed solution which contained 5 mL of
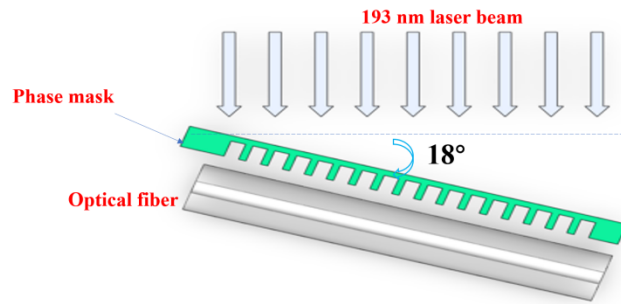
Fig. 1. Phase mask technique for TFBG inscription in an optical fiber.
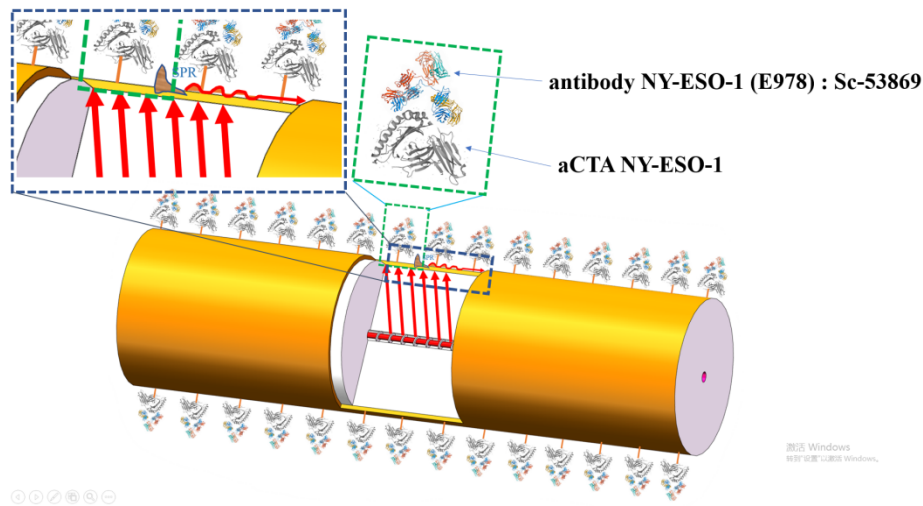
Fig. 2. Schematic diagram of the plasmonic TFBG with functionalized coating.

EDC (0.5 M) and 5 mL of NHS (0.1 M) for 1 hour to activate the carboxyl on the self-assembly of a monolayer. After that, it was rinsed several times with Milli-Q water to remove the unwanted EDC and NHS.

Third, the sensor was immersed in the aCTA NY-ESO-1 solution (0.1 mM) for 135 min to bind the aCTA NY-ESO-1 on the metallic surface. Then, the sensor was immersed in a 3% (w/v) BSA solution for 2 hours to block the excess carboxyl groups. After that, the biosensor was ready for the NY-ESO-1 antibody.

3. Experimental system

Although the spectral evolution of the TFBG-SPR sensor is usually recorded in transmission with both ends of the TFBG connected to a broadband source (BBS) and an optical spectrum analyzer (OSA), respectively, it is difficult for the sensor probe to be functionalized for in-situ detection. Thus, in this work, an Au reflection mirror with a thickness of ~500 nm was deposited on the cleaved extremity of functionalized TFBG. The experimental system for biomolecular measurement is shown in Fig. 3, including a BBS (Golight, ASE C + L LIGHT SOURCE), a polarizer, a polarization controller, a circulator, an TFBG-SPR fiber sensor probe, and an OSA (Anritsu, MS9740A) with a wavelength interval of 0.02 nm for monitoring and recording the full reflected spectra from the functionalized TFBG. In addition, an interrogator (FS22SI Industrial

Bragg METER Interrogator, 1500 nm – 1600 nm, HBM Fiber Sensing) instead of a BBS and an OSA was especially used for dynamic spectrum monitoring with a higher scanning frequency of 1 Hz and a smaller wavelength interval of 0.005 nm. The circulator was used for connecting the biosensor to the OSA or interrogator. The polarizer and the polarization controller were used to control the polarization state of the light launched into the biosensor, ensuring that the launched light worked at the p-polarized state. To reduce, at most, the temperature-induced cross-sensitivity, all the experiments were carried out in a temperature-controlled clean room. Additionally, we should point out here that, during the experiment, the sensor was rinsed with PBS buffer solution for 5 minutes to remove the unbinding biomolecules between different usages.
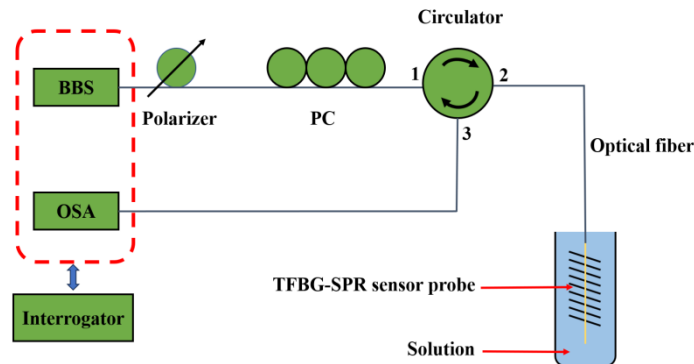

Fig. 3. The experimental system of the plasmonic TFBG biosensor.

4. Results and discussions

4.1. Immobilization of aCTA NY-ESO-1

After the activation of the carboxyl on the self-assembly of a monolayer, the immobilization of aCTA NY-ESO-1 was proceeded. Figure 4 shows the dynamic measured spectra (measured by the OSA) of the proposed biosensor when it was immersed in the aCTA NY-ESO-1 solution. The spectra keep stable except the cladding modes located adjacent to the center of the SPR area, which are sensitive to perturbations near the metallic surface. We selected the most sensitive cladding mode resonance, indicated with a red pentagram "☆" on the left side next to the SPR center, for monitoring the detection procedure. Insets (a) and (b) show, respectively, the responses of the selected cladding mode resonance and the core mode when the biosensor was immersed in a 1.11×10^{-7} M aCTA NY-ESO-1 solution for 135 min. As can be seen, the core mode (Fig. 4(a)) almost kept stable during the immobilization process. It can be understood that the core mode is insensitive to the refractive index but sensitive to the temperature. Therefore, the core mode in the spectrum can be used for calibrating the temperature-induced cross-sensitivity. The selected cladding mode (Fig. 4(b)) is located on the left side of the SPR center, resulting in sensitivity to the variation of the surrounding refractive index (SRI) near the metallic surface. During the immobilization of aCTA NY-ESO-1 on the metallic surface, the SRI increases with time. Therefore, it is obvious that the intensity in the center of the selected cladding mode decreases with time. Note that the optical spectrum analyzer automatically recorded the spectrum every 60 s. Furthermore, it should be pointed out here that, as the biomolecular immobilization and later the biomolecular binding-induced SRI variation are very small, only the intensity variation rather than the wavelength shift in the selected cladding mode can be clearly observed (as shown in Fig. 4(a)). Therefore, throughout this work, we only monitored and discussed the intensity variation of the selected cladding mode.
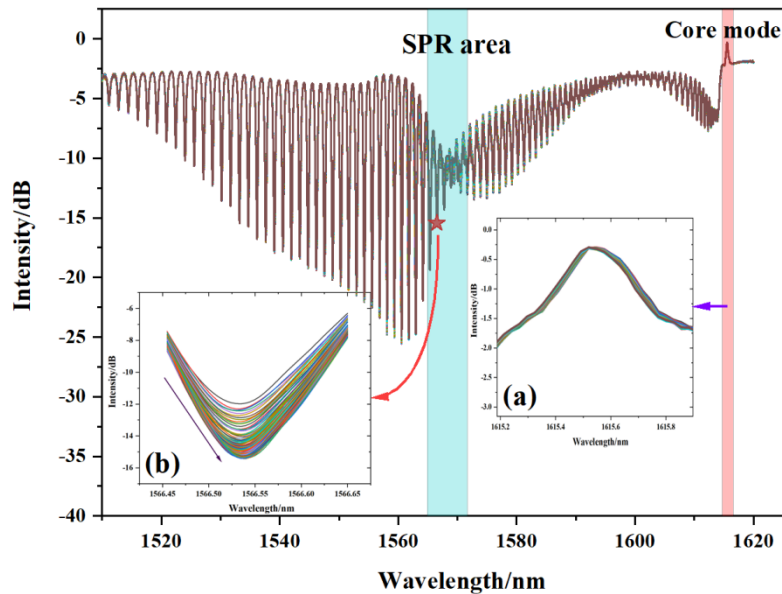
Fig. 4. Measured spectra of the biosensor. Insets (a, b) are, respectively, the responses of the selected cladding mode and core mode when the biosensor is placed in the aCTA NY-ESO-1 solution at a concentration of 1.11×10^{-7} M.

For higher precision, the interrogator was used to focus on the dynamic evolution of a single cladding mode. The immobilization process of aCTA NY-ESO-1 on the metallic surface was followed by monitoring intensity variation of a single cladding mode. To accurately obtain the intensity variation of the selected cladding mode, we applied fitting to the bottom of the selected cladding mode resonance within a range of 2 nm (400 points), and then found the lowest point of intensity. This fitting algorithm is similar to our previous work [23], and it can help find the lowest point easily and quickly.

The monitored signal decreased sharply, showing that the aCTA NY-ESO-1 was quickly bonded on the metallic surface in the first 30 min. Then, it decreased slowly and became stable in the next 30 min, which means that the bio-functionalization was complete within 60 min. The decrease of the cladding mode intensity corresponds to the increase of the surrounding refractive index [24]. After the immobilization of aCTA NY-ESO-1, the biosensor needs to be encapsulated with BSA to block the excess carboxyl groups before the detection of NY-ESO-1 antibody, improving the protein stability and preventing non-specific binding. The encapsulation process of BSA on the biosensor is also shown in Fig. 5. (a), and it is obvious that the induced intensity variation is far smaller than the immobilization of aCTA, which means most of the functional groups on the surface of the biosensor have already bound to the aCTA. Furthermore, to demonstrate the repeatability, we repeated the immobilization of aCTA three times and the results are shown in Fig. 5. (b). The signal variation (with a variance of ~2.3 dB) caused by the aCTA immobilization is much larger than that caused by the BSA (with a variance of ~0.5 dB), which verifies the feasibility of our method for preparing the biosensor.

4.2. Detection of NY-ESO-1 antibody

In order to further demonstrate the performance of the biosensor for measuring NY-ESO-1 antibody in different concentrations and verify the feasibility of the proposed biosensor for detection of NY-ESO-1 antibody, experiments were carried out with NY-ESO-1 antibody in
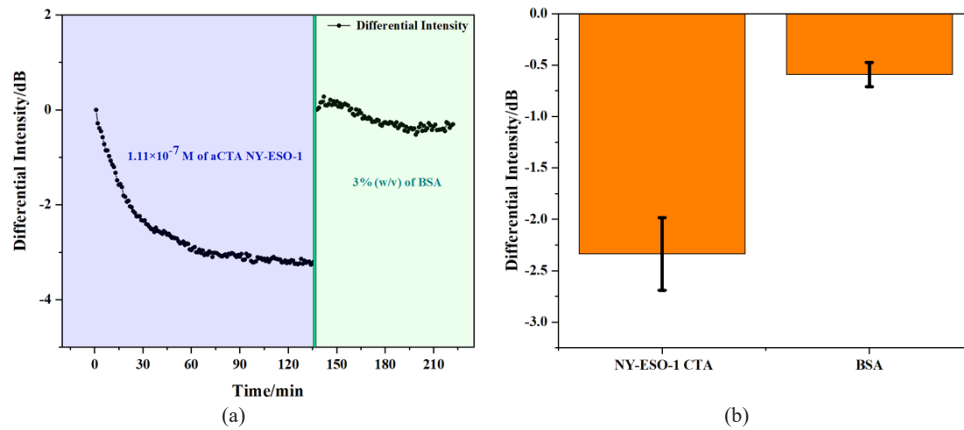
Fig. 5. (a) The intensity variation of the selected cladding mode during the immobilization of aCTA NY-ESO-1 (1.11×10^{-7} M) on the metallic surface and the 3%(w/v) BSA adsorption; (b) The 3-time measurement for the immobilization of the aCTA NY-ESO-1 and the BSA.

concentrations of 2×10^{-7}, 2×10^{-6}, 2×10^{-5}, 2×10^{-4}, 2×10^{-3} and 2×10^{-2} µg/ml. In general, the intensity of the selected cladding mode increases as a function of time. This phenomenon is opposite to the counterparts for the antigen and the BSA adsorption, as shown in Fig. 5, which could be related to the structure changes on the fiber surfaces [25]. When the concentrations are 2×10^{-6} and 2×10^{-5} µg/ml, the trends of intensity variations are similar to that of 2×10^{-7} µg/ml but with saturated values increased with the concentration, as shown in Fig. 6. (a). The trend of the variation is very regular, which agrees with the theory of combination between a pair of antibodies and antigens. The detected signal becomes almost stable after 30 min, which means that the interaction between the aCTA NY- ESO-1 and NY-ESO-1 antibody reaches equilibrium. Figure 6. (b) and Fig. 6. (c) present the second and third measured results of NY-ESO-1 antibody by in concentrations of 2×10^{-7}, 2×10^{-6}, and 2×10^{-5} µg/ml, which are the same trend as the first measurement. Figure 6. (d) shows the linear fit of the measured results in concentrations of 2×10^{-7}, 2×10^{-6}, and 2×10^{-5} µg/ml and the relationship between the saturated values (obtained from the first and the second measurement) in measured time of 15, 20, and 25 min. It can be calculated that the linearity is 99.9%, which means that our biosensor has a measured range from 2×10^{-7} to 2×10^{-5} µg/mL. It is worth noting that the measured method used in this work is from low to high concentration [17,26]. Despite the fact that just three concentrations are displayed in Fig. 6, the variation in signal intensity will continue to rise with concentration until the hook effect (seen in Fig. 8) appears.

Figure 7 depicts a microscopic view of the biosensor's surface before and after detection. The metallic surface was smooth (locally expanded picture displayed on the right side of Fig. 7(a)) before detection and rough (locally enlarged image shown on the right side of Fig. 7(b)) after detection of the NY-ESO-1 antibody. The strip in dark gray shown in the locally magnified picture on the right side of Fig. 7(b) was the NY-ESO-1 antibody captured by the biosensor.

Figure 8. (a) shows the intensity variation of the selected cladding mode with the concentrations of NY-ESO-1 antibody at 2×10^{-4}, 2×10^{-3} and 2×10^{-2} µg/ml. It is found that the intensity of the selected cladding mode is not sensitive to the PBS. For 2×10^{-4} µg/ml, the intensity variation increases to 0.4 dB, and then an obvious decrease is observed. For 2×10^{-3} µg/ml, a large intensity variation of ~1 dB is obtained. However, the intensity variation abnormally decreases to ~0.6 dB for 2×10^{-2} µg/ml without increasing with concentration. This phenomenon may be caused by the hook effect. The hook effect, also known as the high-dose hook effect or the prozone effect, is a phenomenon that occurs in biomolecular detection assays [27,28]. The hook
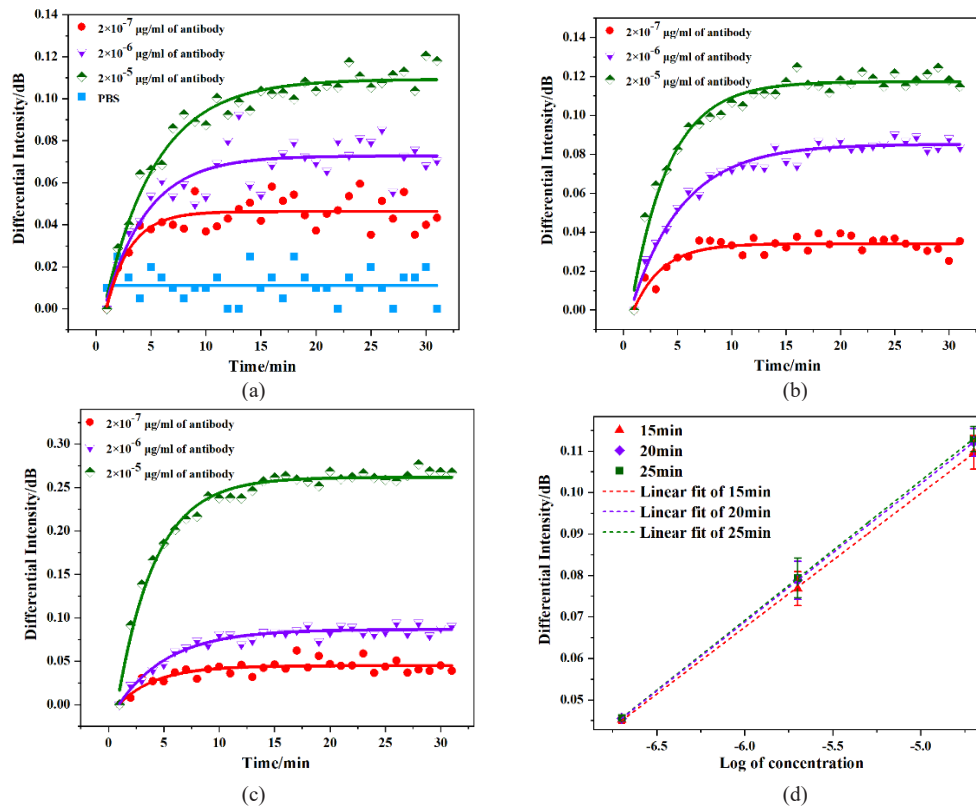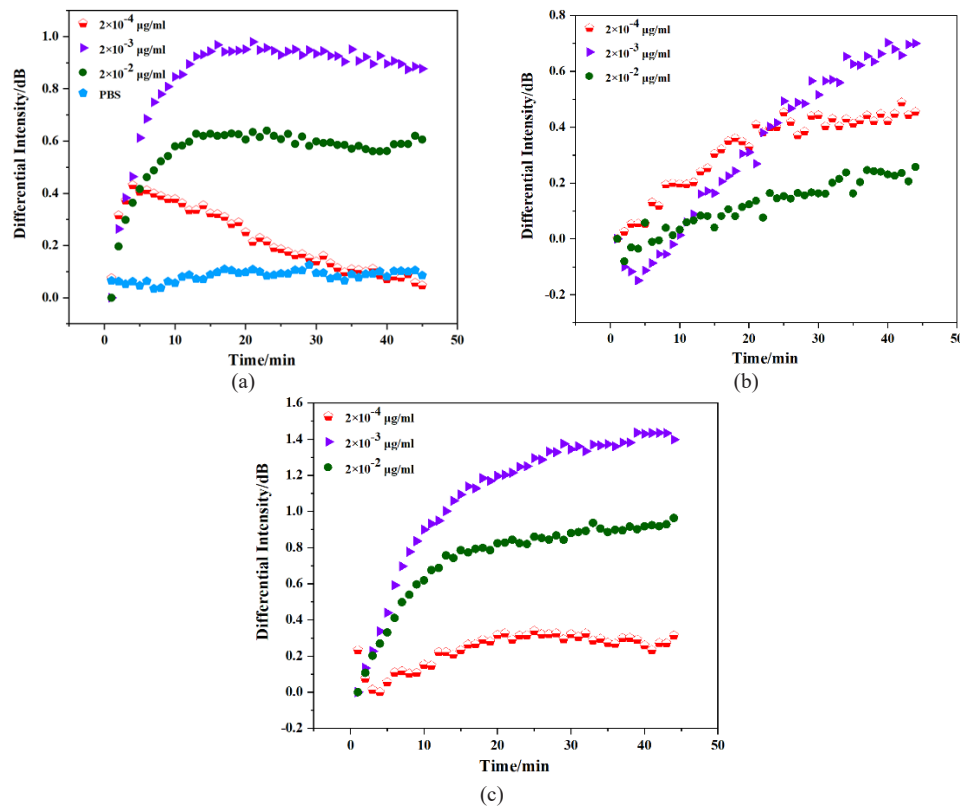
Fig. 6. The measured results of NY-ESO-1 antibody in concentrations of 2×10^{-7}, 2×10^{-6}, and 2×10^{-5} µg/ml in three times: (a) first time, (b) second time, (c) third time; and (d) the relationship between the saturated values and the concentrations in three measurable time (15, 20, and 25 min).
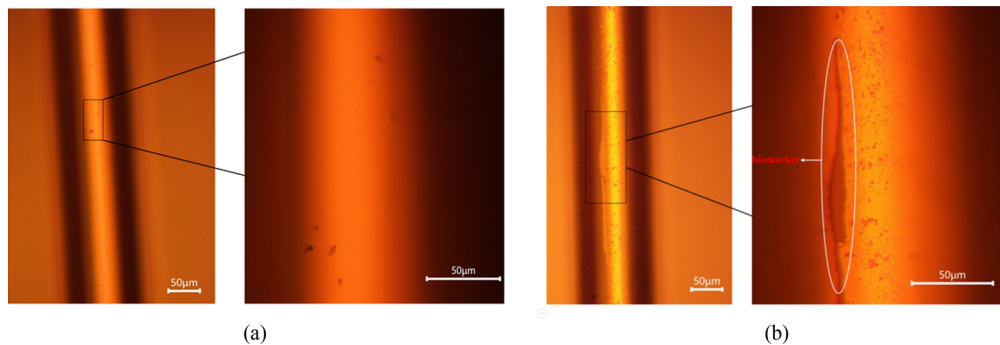
Fig. 7. Microscopic view of the biosensor surface before (a) and after (b) the detection. The images on the right side of (a) and (b) are the locally enlarged pictures.

effect can also be observed in other biological processes, such as bacterial agglutination [29], hemagglutination assays [30], and mixed hemadsorption [31]. In this work, it could happen when the concentration of the target molecule (e.g., NY-ESO-1 antibody in this work) in a sample becomes so high that it exceeds the detection limit of the assay.

Fig. 8. The measured results of NY-ESO-1 antibody in concentrations of 2×10^{-4}, 2×10^{-3}, and 2×10^{-2} µg/ml in three times: (a) first time, (b) second time, and (c) third time.

When the concentration is 2×10^{-2} µg/ml, the total amount of NY-ESO-1 antibody in the solution is larger than aCTA NY-ESO-1 on the metallic surface, and the excess amount can saturate the available binding sites on the probes. Furthermore, due to biomolecular competition at high concentrations, some of the NY-ESO-1 antibodies cannot get close to the binding sites on the aCTA NY-ESO-1, resulting in low binding efficiency. As a result, the antibody-antigen combination is hindered or disrupted, leading to a decreased or absent signal. This can lead to a false-negative result in the assay, where the actual presence of the target molecule is not detected.

To further prove the possibility of the hook effect, this experiment was repeated twice for NY-ESO-1 antibody measurement from low to high concentration. Although similar trends with the hook effect are shown, the evolutions of the intensity at the same concentration behave differently for the three experiments, showing that the biosensor is less repetitive at higher concentrations from 2×10^{-4} to 2×10^{-2} µg/ml than lower concentrations from 2×10^{-7} to 2×10^{-5} µg /mL. It is worth noting that the hook effect can be overcome by diluting the sample to reduce the concentration of the target molecule, which enables a more even distribution of excess target molecules and allows for antibody-antigen binding and accurate detection.

5. Conclusion

We have proposed and experimentally demonstrated a functionalized TFBG for NY-ESO-1antibody detection and the results, obtained through intensity interrogation, show that our biosensor can provide a LOD at a concentration of 2×10^{-7} µg/ml, and with good linearity in

the measured range from 2×10^{-7} to 2×10^{-5} μg/ml. The experimental results also indicate a hook effect when the NY-ESO-1 antibody concentration is higher than 2×10^{-3} μg/ml. Owing to the hook effect, the effective measurable range of our biosensor is 2×10^{-7}- 2×10^{-3} μg/ml. The TFBG-SPR sensor presented in this paper has the advantages of excellent performance, a simple structure, a simple preparation method, and a compact size, making it an ideal tool for in situ, unlabeled and subscale detection (interactions of organisms at the nanoscale) of NY-ESO-1 antibody (with aCTA NY-ESO-1 serving as probes) and other biomolecules (with related specific molecules serving as probes). Additionally, the core mode, monitored using an OSA together with a BBS, in the TFBG spectrum can be used to calibrate cross-sensitivity caused by temperature and power fluctuations, thereby improving measurement accuracy [32].

References

1. C.S. Chung, Y. C. Lee, C. P. Wang, J. Y. Ko, W. L. Wang, M. S. Wu, and H. P Wang, "Secondary prevention of esophageal squamous cell carcinoma in areas where smoking, alcohol, and betel quid chewing are prevalent," J Formos Med Assoc. **109**(6), 408–421 (2010).
2. R. J Kelly, "Emerging Multimodality Approaches to Treat Localized Esophageal Cancer," J Natl Compr Canc Netw. **17**(8), 1009–1014 (2019).
3. J. R. Siewert, U. Fink, K. T. Beckurts, and J. D Roder, "Surgery of squamous cell carcinoma of the esophagus," Ann Oncol. **5**(Suppl 3), 1–7 (2014).
4. Y. W. Xu, Y. H. Peng, and B. Chen, *et al.*, "Autoantibodies as potential biomarkers for the early detection of esophageal squamous cell carcinoma," Am J Gastroenterol. **109**(1), 36–45 (2014).
5. Y. He, S. Ren, K. Suda, C. Rivard, Y. Wang, X. Li, C. Zhou, and F. R Hirsch, "Tumor autoantibodies (TAAs) panel can improve the accuracy of early diagnosis in lung cancer presenting with ground-glass nodules (GGNs) in Chinese population. Lung Cancer. 2018. In press.
6. G. Sun, H. Ye, Q. Yang, J. Zhu, C. Qiu, J. Shi, L. Dai, K. Wang, J. Zhang, and P Wang, "Using proteome microarray and gene expression omnibus database to screen tumour-associated antigens to construct the optimal diagnostic model of oesophageal squamous cell carcinoma," Clinical Oncology. **35**(10), e582–e592 (2023).
7. M. Wang, F. Liu, and Y. Pan, *et al.*, "Tumor-associated autoantibodies in ESCC screening: Detecting prevalent early-stage malignancy or predicting future cancer risk?" EBioMedicine. **73**, 103674 (2021).
8. T. Kakimoto, A. Matsumine, S. Kageyama, K. Asanuma, T. Matsubara, T. Nakamura, T. Iino, H. Ikeda, H. Shiku, and A Sudo, "Immunohistochemical expression and clinicopathological assessment of the cancer testis antigens NY-ESO-1 and MAGE-A4 in high-grade soft-tissue sarcoma," Oncology letters. **17**, 3937–3943 (2019).
9. W. Shi, Z. Tong, Q. Qiu, N. Yue, W. Guo, F. Zou, D. Zhou, J. Li, W. Huang, and H Qian, "Novel HLA-A2 restricted antigenic peptide derivatives with high affinity for the treatment of breast cancer expressing NY-ESO-1," Bioorg Chem. **103**, 104138 (2020).
10. S. Fujita, H. Wada, and A. A. Jungbluth, *et al.*, "NY-ESO-1 expression and immunogenicity in esophageal cancer," Clinical cancer research : an official journal of the American Association for Cancer Research. **10**(19), 6551–6558 (2004).
11. S. Gnjatic, H. Nishikawa, A. A. Jungbluth, A. O. Güre, G. Ritter, E. Jäger, A. Knuth, Y. T. Chen, and L. J Old, *NY-ESO-1: Review of an Immunogenic Tumor Antigen. Advances in Cancer Research*, Academic Press. 95, 1–30 (2006).
12. S. Hosseini, P. Vázquez-Villegas, M. Rito-Palomares, and S.O. Martinez-Chapa, *Advantages, Disadvantages and Modifications of Conventional ELISA. Enzyme-linked Immunosorbent Assay (ELISA): From A to Z*. S. Hosseini,

P. Vázquez-Villegas, M. Rito-Palomares, and S. O. Martinez-Chapa, eds. Singapore, Springer Singapore, 2018, 67–115.11

13. X. Chen, J. Xu, X. Zhang, T. Guo, and B.O Guan, "Wide Range Refractive Index Measurement Using a Multi-Angle Tilted Fiber Bragg Grating," IEEE Photonics Technology Letters. **29**(9), 719–722 (2017).

14. T. Guo, F. Liu, B.-O. Guan, and J Albert, "Tilted fiber grating mechanical and biochemical sensors," Optics & Laser Technology. **78**, 19–33 (2016).

15. H.-Y. Wen, Y.-C. Hsu, S.-Y. Chen, and C.-C Chiang, "The manufacturing process and spectral features of tilted fiber Bragg gratings," Optics & Laser Technology. **134**, 106615 (2021).

16. M. Piliarik and J Homola, "Surface plasmon resonance (SPR) sensors: approaching their limits?" Opt. Express **17**(19), 16505–1651 (2009).

17. W. Udos, C.-W. Ooi, S.-H. Tan, K.-S. Lim, Y. J. Ee, K. C. Ong, and H Ahmad, "Label-free surface-plasmon resonance fiber grating biosensor for Hand-foot-mouth disease (EV-A71) detection," Optik. **228**, 166221 (2021).

18. M. Loyez, E. M. Hassan, M. Lobry, F. Liu, C. Caucheteur, R. Wattiez, M. C. DeRosa, W. G. Willmore, and J Albert, "Rapid Detection of Circulating Breast Cancer Cells Using a Multiresonant Optical Fiber Aptasensor with Plasmonic Amplification," ACS sensors. **5**(2), 454–463 (2020).

19. L. Liu, X. Zhang, Q. Zhu, K. Li, Y. Lu, X. Zhou, and T. Guo, "Ultrasensitive detection of endocrine disruptors via superfine plasmonic spectral combs," Light, Sci Appl. **10**(1), 181 (2021).

20. X. Chen, P. Xu, W. Lin, J. Jiang, H. Qu, X. Hu, J. Sun, and Y Cui, "Label-free detection of breast cancer cells using a functionalized tilted fiber grating," Biomed Opt Express. **13**(4), 2117–2129 (2022).

21. T. Sakane, T. Murase, K. Okuda, A. Masaki, R. Nakanishi, and H Inagaki, "Expression of cancer testis antigens in thymic epithelial tumors," Pathol Int. **71**(7), 471–479 (2021).

22. C. Ribaut, M. Loyez, J. C. Larrieu, S. Chevineau, P. Lambert, M. Remmelink, R. Wattiez, and C Caucheteur, "Cancer biomarker sensing using packaged plasmonic optical fiber gratings: Towards in vivo diagnosis," Biosens Bioelectron. **92**, 449–456 (2017).

23. W. Lin, W. Huang, Y. Liu, X. Chen, H. Qu, and X Hu, "Cladding Mode Fitting-Assisted Automatic Refractive Index Demodulation Optical Fiber Sensor Probe Based on Tilted Fiber Bragg Grating and SPR," Sensors. **22**, 3032 (2022).

24. C. Caucheteur, V. Voisin, and J Albert, "Polarized spectral combs probe optical fiber surface plasmons," Opt Express. **21**(3), 3055–3066 (2013).

25. K. Tomyshev, E. I. Dolzhenko, A. D. Vasilyeva, L. V. Yurina, and O. V Butov, "Selective fiber optic TFBG-assisted biosensors featuring functional coatings," Sensors and Actuators B: Chemical. **384**, 13361 (2023).

26. W Yang, Y. Cheng, M Jiang, S. Jiang, R Liu, J Lu, L Du, P, Li, and C Wang, "Design and fabrication of an ultra-sensitive Ta2C MXene/Au-coated tilted grating sensor," Sensors and Actuators B: Chemical. **369**, 132391 (2022).

27. J. Chen, K.-H. Chen, L.-M. Wang, W.-W. Zhang, L. Feng, H.-Z. Dai, and Y.-N He, "High-dose HOOK effect in urinary DcR2 assay in patients with chronic kidney disease," Clinical Biochemistry. **58**, 32–36 (2018).

28. K. Papik, B. Molnar, P. Fedorcsak, R. Schaefer, F. Lang, L. Sreter, J. Feher, and Z Tulassay, "Automated Prozone Effect Detection in Ferritin Homogeneous Immunoassays Using Neural Network Classifiers," Clin Chem Lab Med. **37**(4), 471–476 (1999).

29. BH Buxton, "Bacteriolytic Power of Immune Serum and the Theory of Complement Diversion," J Med Res. **13**, 431–459 (1905).

30. A. Townsend, P. Rijal, and J. Xiao, *et al.*, "A haemagglutination test for rapid detection of antibodies to SARS-CoV-2," Nat Commun. **12**, 1951 (2021).

31. E. Linder and A Miettinen, "Prozone effects in indirect immunofluorescence," Scand J Immunol. **5**(5), 513–519 (1976).

32. D Harasim, "Polatization-insensitive refractive index measurement using cascaded perpendicular tilted fiber Bragg gratings," Measurement. **202**, 111845 (2022).